PAPER • OPEN ACCESS

Ultrafast carrier dynamics at organic donor–acceptor interfaces—a quantum-based assessment of the hopping model

To cite this article: Maximilian F X Dorfner *et al* 2022 *J. Phys. Mater.* **5** 024001

View the article online for updates and enhancements.

Journal of Physics: Materials

PAPER

OPEN ACCESS

Ultrafast carrier dynamics at organic donor–acceptor interfaces—a quantum-based assessment of the hopping model

Maximilian F X Dorfner[1], Sebastian Hutsch[1], Raffaele Borrelli[2] , Maxim F Gelin[3] and Frank Ortmann[1],*

1 Department of Chemistry, Technische Universität München, 85748 Garching b. München, Germany
2 DISAFA, University of Torino, Largo Paolo Braccini 2, I-10095 Grugliasco, TO, Italy
3 School of Sciences, Hangzhou Dianzi University, Hangzhou 310018, People's Republic of China
* Author to whom any correspondence should be addressed.
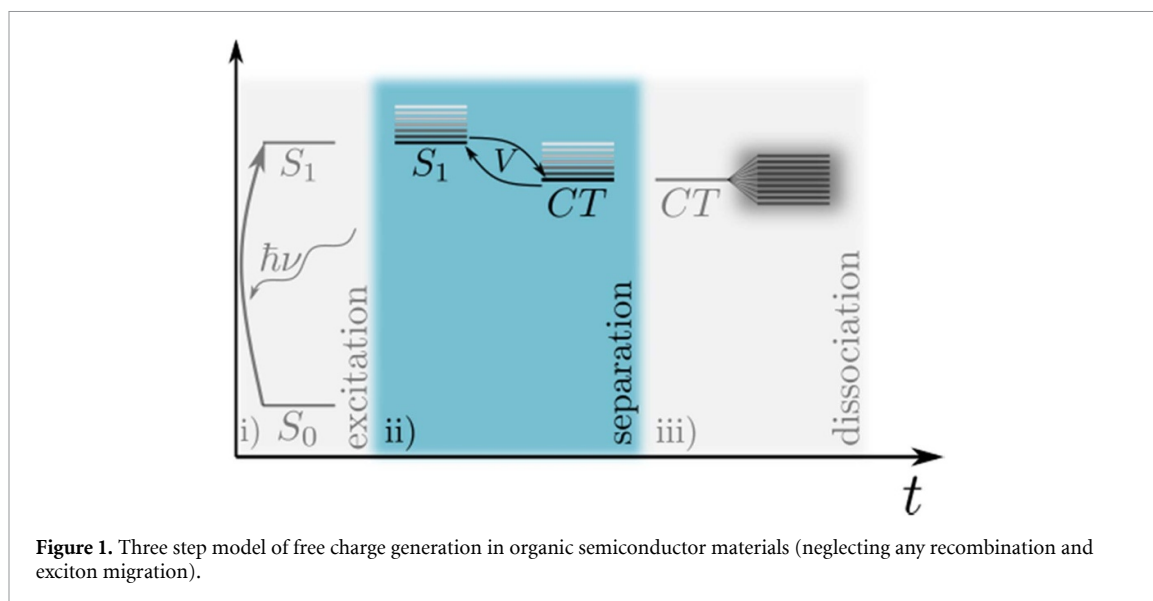
E-mail: frank.ortmann@tum.de

Abstract

We investigate the charge transfer dynamics of photogenerated excitons at the donor–acceptor interface of an organic solar cell blend under the influence of molecular vibrations. This is examined using an effective Hamiltonian, parametrized by density functional theory calculations, to describe the full quantum behaviour of the relevant molecular orbitals, which are electronically coupled with each other and coupled to over 100 vibrations (via Holstein coupling). This electron–phonon system is treated in a numerically quasi-exact fashion using the matrix-product-state (MPS) ansatz. We provide insight into different mechanisms of charge separation and their relation to the electronic driving energy for the separation process. We find ultrafast electron transfer, which for small driving energy is dominated by kinetic processes and at larger driving energies by dissipative phonon emission connected to the prevalent vibration modes. Using this fully quantum mechanical model we perform a benchmark comparison to a recently developed semi-classical hopping approach, which treats the hopping and vibration time scales consistently. We find qualitatively and quantitatively good agreement between the results of the sophisticated MPS based quantum dynamics and the simple and fast time-consistent-hopping approach.

1. Introduction

Organic molecular blends based on fullerene acceptors (FAs), have been in the focus of intensive research efforts in the organic solar cell community, due to their reliable performance in the solar energy conversion [1, 2]. Despite the recent advent of non-fullerene acceptor systems [3, 4] with power conversion efficiencies reaching 18% [5], FA-based blends remain important model systems to study key electronic and optoelectronic processes and limiting factors of organic photovoltaic devices [6–12].

The photogeneration of charges in organic solar cells is believed to be a three step process [13], reflecting the time scale separation on which these processes occur. These steps are (i) the photogeneration of a local excitonic singlet state (S_1) above the ground state (S_0) together with its possible migration to the donor–acceptor interface, (ii) the separation of the electron and the hole at the interface into a so-called charge transfer (CT) state and (iii) the dissociation into free carriers (cf figure 1) [14]. The intermediate CT states formed by electron transfer from the donor to the acceptor are precursors to fully separated charges. In photovoltaics they have been assigned a key role [15] because the open circuit voltage crucially depends on such states [16]. Therefore they have been studied intensively [10, 17–20].

Among a larger set of possible parameters [21, 22], the time scale at which this transfer happens (or its inverse the CT rate), impacts the charge generation process and therefore influences the power conversion efficiency of the solar cell. This rate is not only affected by the transfer integrals and the energy difference (driving energy) between the involved lowest unoccupied molecular orbitals (LUMO) of the transfer process,

Figure 1. Three step model of free charge generation in organic semiconductor materials (neglecting any recombination and exciton migration).

as extensively studied previously [14, 23–25], but due to the large number of atomic constituents, also by a huge number of electronically coupled vibrations (phonon modes).

This CT has been analysed in terms of hopping models assuming almost vanishing electronic coupling [26], which is justified for localized states. In absence of delocalized band states in disordered organic semiconductors, this seems a plausible assumption. From a theoretical point of view the transfer rates for these systems are commonly calculated semi-classically by employing the Marcus hopping (MH) theory [27, 28] or a Levich–Jortner hopping (LJH) approach [29], which give more or less reasonable results compared to experiments, but suffer from conceptual problems. For example coherence effects and tunnelling are *a priori* not (or only to a limited degree) contained in the MH and LJH theories. Furthermore it is usually assumed that the phonon modes can be treated quasi-classically (citing the condition: $\hbar\omega \ll k_{B}T$, where ω is the phonon frequency, $\hbar$ the reduced Planck constant, k_{B} Boltzmann's constant, and T the absolute temperature), which is not always the case or satisfied only for a limited number of phonon modes. In addition it is assumed that the system remains in a (quasi-)equilibrium during the transfer process, which is also questionable [26]. On more fundamental grounds, both MH and LJH approaches usually do not treat the intrinsic time scales of the problem consistently [30]. For example phonon modes with low energy are frequently included in a dynamic treatment, although the time scale of the CT dynamics is much shorter than the time scale on which the phonon modes oscillate and for which a quasi-static treatment would be more appropriate. But progress has been made to resolve this issue. To restore the internal consistency of time and energy scales, self-consistency conditions have been proposed [31, 32], which has recently led to the development of a time-consistent hopping (TCH) approach [30]. The basic idea of this approach is the self-consistent determination of the hopping rate and a cutoff energy scale separating the fast dynamical and the slow (quasi-) static treatment of the modes.

In addition to the MH, LJH and TCH theories, there are a number of other approaches that investigate the influence of phonons on the properties of organic solar cells. These are, among others [33, 34], based on Ansatz wave functions [35], a dynamics controlled truncation scheme within the density matrix formalism [36], Green's function formalism [37] or the quantum master equation [38]. Despite their success in describing some of the aspects characteristic for electron–phonon coupled systems, these approaches usually suffer from the curse of dimensionality, i.e. they can only take into account a very limited number of phonon modes explicitly.

In order to assess the role of molecular vibrations for the charge-transfer process and to provide exact benchmark simulations for comparison with simpler and faster hopping models, we analyse the quantum dynamics in an unbiased approach, for which a separation into the analytic limits is not necessary. This is achieved by simulating the vibronically coupled carrier dynamics, with a non-perturbative fully quantum mechanical matrix product state (MPS) approach, applied to an effective model that is parametrized by density functional theory calculations. Although other authors [39] have also taken into account the effect of non-local electron–phonon coupling on the transport and optical properties of organic semiconductors, we restrict ourselves to a Holstein coupling.

Here we focus on a diketopyrrolopyrrole (DPP)–fullerene derivative (PC[70]BM) blend system [40], in which pump-probe experiments revealed that the dynamics on short timescales (<1 ps) after excitation is

governed by the S_1 and the CT states. We study the role of the energetic offset between the S_1 and CT states ('driving energy') and find that for a matching energy between the most strongly coupled phonon modes and the electronic energy difference, the CT process can be accelerated, which could be beneficial for the efficiency of a solar cell device. Furthermore, we compare the CT time obtained by this numerically exact approach with the TCH approach. Although both approaches *a priori* treat the problem on rather different footings, we find remarkably good agreement in the absolute values of the rates and their dependencies on the driving energy.

2. Methodology

2.1. Model and quantity of interest

We restrict ourselves to the process of the initial CT from the photo-excited, fully localized $|S_1\rangle$ state to the charge transfer state $|CT\rangle$. The hole generated on the donor site is regarded as immobile, as considered in previous work [35]. We note that the authors of [41] have found that this assumption may lead to a reduction of the total transferred charge density by studying a chain-model of a donor–acceptor system and neglecting molecular vibrations. A multilayer multiconfiguration time-dependent Hartree study was able to take into account the effect of the vibrations and a restricted set of electron–hole states quantum mechanically on a similar system [42], however, the focus of the study was not to elaborate on the interplay between electron–hole attraction and electron–phonon coupling, such that this question remains a topic for further investigations. Owing to the assumption that the excitation process is much faster than the charge separation (separation of timescales), we neglect possible time dependencies of the Hamiltonian due to the excitation process or other non-equilibrium effects. Likewise, a complete excitation from the ground state is conjectured.

We consider that the initial exciton is generated directly at the interface (absence of exciton diffusion). This means that the initial electronic state of the system is the pure $|S_1\rangle$ state, whereas each of the molecular phonon modes is in a (decoupled) equilibrium configuration, such that the initial state is given by

$$\rho_0 = |S_1\rangle\langle S_1| \otimes \rho_1 \otimes \rho_2 \otimes \ldots \otimes \rho_N,$$

where $\rho_i = \frac{1}{Z_i(\beta)} \sum_{n_i=0}^{\infty} e^{-\beta\hbar\omega_i n_i} |n_i\rangle\langle n_i|$, $Z_i(\beta)$ is the canonical partition sum of the decoupled mode i and $\beta = (k_B T)^{-1}$.

After the excitation process this initial state evolves under the dynamics of the coupled electron–phonon system. Here we restrict ourselves to a local electron–phonon coupling, i.e. we exclusively consider molecular vibrations, which couple either to $|S_1\rangle$ or $|CT\rangle$. Within these assumptions the Hamiltonian under consideration is given by

$$H = H_{\text{el}} + H_{\text{el-ph}} + H_{\text{ph}}$$

where

$$H_{\text{el}} = V|S_1\rangle\langle CT| + V|CT\rangle\langle S_1| + \Delta E|CT\rangle\langle CT|,$$

denotes the electronic part of the Hamiltonian with V the transfer integral between the state
$|S_1\rangle$ of the DPP donor (cf figure 2) and the electronic CT state $|CT\rangle$, where ΔE is the electronic driving energy of the system. The second term,

$$H_{\text{el-ph}} = \sum_{\lambda} g_{\lambda}|S_1\rangle\langle S_1|\left[a_{\lambda} + a_{\lambda}^{\dagger}\right] + \sum_{\mu} h_{\mu}|CT\rangle\langle CT|\left[b_{\mu} + b_{\mu}^{\dagger}\right],$$

describes the (local) coupling between the phonon modes and the electronic states and

$$H_{\text{ph}} = \sum_{\lambda} \hbar\omega_{\lambda} a_{\lambda}^{\dagger} a_{\lambda} + \sum_{\mu} \hbar\nu_{\mu} b_{\mu}^{\dagger} b_{\mu},$$

is the energy contribution from the phonons. Here, a_{λ} and b_{μ} denote the bosonic annihilation operators for the respective site, h_{μ} and g_{λ} are the electron–phonon coupling matrix elements for the fullerene derivative and the polymer sites, respectively, and ν_{μ} and ω_{λ} are the corresponding phonon frequencies.

Here we are interested in the time scale upon which the CT occurs for this polymer-fullerene blend system. For this purpose we compute the population of $|S_1\rangle$ over time

Figure 2. Relation between the model system and the specific electronic donor–acceptor system. Here 'GS' denotes the ground state of the respective molecular component, i.e. of the donor or the acceptor, whereas 'S_0' in figure 1 denotes the ground state of the combined system.
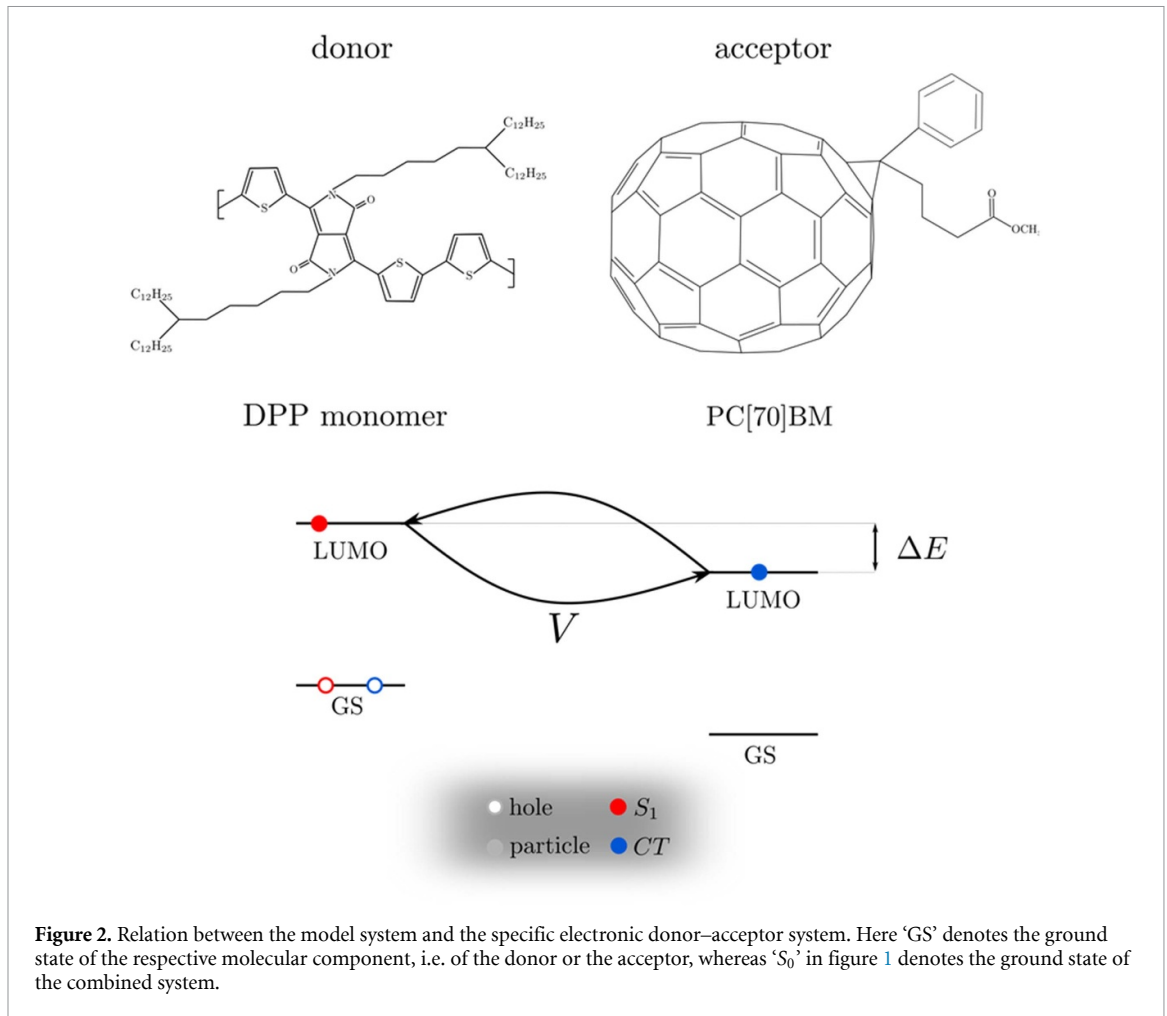
$$p_{S_1}(t) = \langle P_{S_1}(t) \rangle = tr\left(\rho_0 e^{iHt/\hbar} P_{S_1} e^{-iHt/\hbar} \right),$$
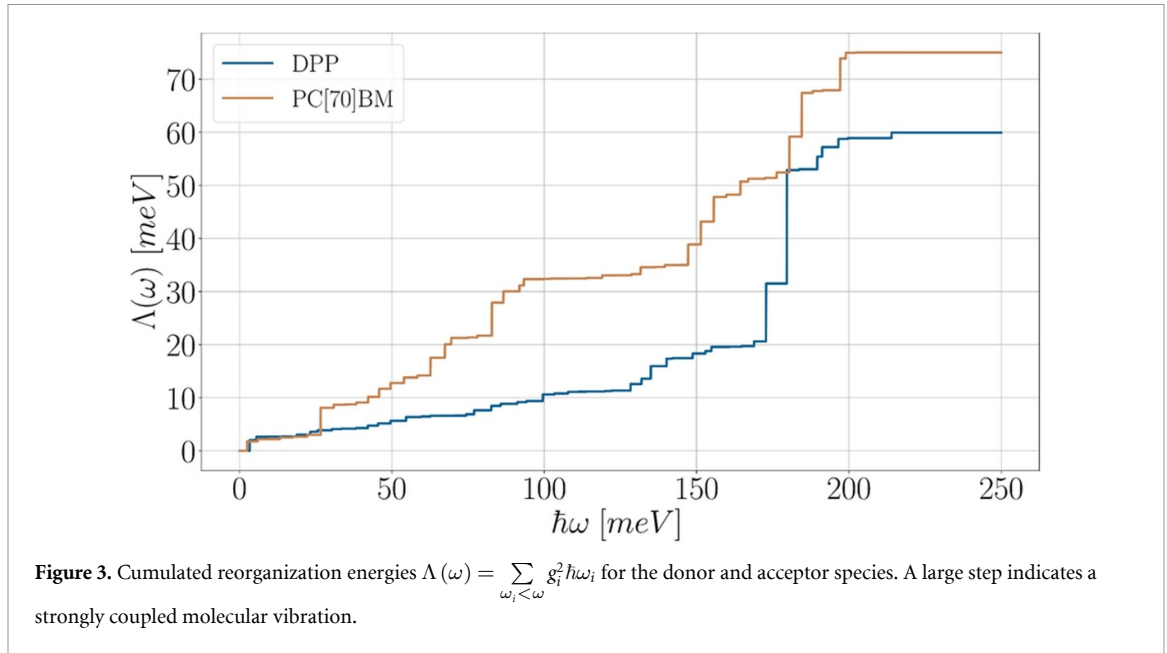
where $P_{S_1} = |S_1\rangle \langle S_1| \otimes 1 \otimes 1 \otimes \ldots \otimes 1$, the projector to the electronic factor space.

2.2. *Ab initio* parametrization of the model

In order to describe the considered blend specifically, the model is parametrized by density functional theory (DFT) calculations. The transfer integral between the S_1 state and the CT state has been estimated, after initial geometry optimizations as described in [40], within the fragmented orbital approach [43] between the LUMO of the PC[70]BM and the LUMO of the DPP polymer, by employing the B3LYP functional [44, 45] and the 6-311G** basis set [46] as implemented in the Gaussian 16 software package. The transfer integrals of the frontier orbitals are in a range of 20 meV to 40 meV depending on the orientation of the two molecules to each other. In this study we consider the representative value of $V = 25$ meV. Since we assume the localized hole on the donor to be immobile we just consider the LUMO orbitals of the corresponding molecular units. This relation between the electronic part of our model system and the DFT calculation is illustrated schematically in figure 2. To access the vibration spectrum a normal mode analysis [47] is performed using the 6-311G** basis set and the B3LYP functional as implemented in Gaussian 16. The electron–phonon coupling matrix elements have been computed as derivatives of the Kohn–Sham energies of the LUMO's of the respective molecular structure with respect to the normal coordinates of the phonon modes [48]. We consider in each of our calculations the initial temperature of the phonon modes to be $k_B T = 25$ meV.

2.3. Coarse graining of the phonon modes

To cope with the large number of effectively coupled modes we reduce the overall 803 modes obtained by the DFT procedure by a coarse graining method that is performed as follows: We sample the frequency axis up to

Figure 3. Cumulated reorganization energies $\Lambda(\omega) = \sum\limits_{\omega_i < \omega} g_i^2 \hbar\omega_i$ for the donor and acceptor species. A large step indicates a strongly coupled molecular vibration.

the largest phonon frequency with a grid of intervals $I_i = [\omega_i; \omega_{i+1}]$, $i = 1, \ldots, N$, of size $\Delta\omega = \omega_{i+1} - \omega_i$. Each interval defines an effective mode with a coupling constant

$$g_i^2 = \sum_{\omega_\lambda \in I_i} g_\lambda^2,$$

and a frequency

$$\omega_i = \frac{1}{g_i^2} \sum_{\omega_\lambda \in I_i} \omega_\lambda g_\lambda^2,$$

respectively for the modes of the fullerene derivative. The grid spacing $\Delta\omega$ determines the quality of the effective model. As a compromise between accuracy and computational cost, we set $\Delta\omega = 4$ meV. This results in 57 effective phonon modes ranging from $\hbar\omega_1 \approx 3.3$ meV to $\hbar\omega_{57} \approx 408$ meV. An analogous procedure is performed for the fullerene derivative, which results in 114 effective modes in total.

The coarse grained mode spectrum resembles qualitatively the original normal mode spectrum. These modes contribute to the reorganization energy $\Lambda(\omega)$ of the respective molecular part which (co-)determines the dynamics of the carrier on the different time scales of the CT process. A comparison between the reorganization energies for the two species can be found in figure 3. The acceptor molecule is dynamically favoured, due to a larger polaronic on-site energy shift of the high-energy modes for the fullerene derivative. The modes with lower energy (<25 meV) have a similar impact on the reorganization energy for both sites.

2.4. A brief overview to MPS techniques

To perform the time evolution and compute the expectation values as described above we make use of a MPS formulation of the problem. While it is not the scope of this article to give a detailed introduction into the extensive MPS methodology, we still want to give a brief idea, how this method works and which limitations a prospective adopter of the method might face. For the interested reader we refer to the review articles [49, 50] and [51].

The MPS methodology offers a way to study correlated quantum many-body systems in a numerically quasi-exact fashion, without explicitly diagonalizing the exponentially hard problem. It is based on the ansatz states, which can be written in the form

$$|\phi\rangle = \sum_{\sigma_1, \ldots, \sigma_N} A^{\sigma_1} \cdot A^{\sigma_2} \cdot \ldots \cdot A^{\sigma_N} |\sigma_1\rangle \otimes |\sigma_2\rangle \otimes \ldots \otimes |\sigma_N\rangle,$$

where A^{σ_i} are complex valued matrices of suitable size, which depend only on the state $|\sigma_i\rangle$ within the so called local Hilbert space spanned by the orthonormal basis $\{|\sigma_i\rangle\}$ [49, 52]. In our case a local Hilbert space

is either the bare electronic space or the space spanned by the occupation number states of mode *i*. This ansatz amounts in approximating a quantum state

$$|\psi\rangle = \sum_{\sigma_1,\ldots,\sigma_N} C^{\sigma_1,\ldots,\sigma_N} |\sigma_1\rangle \otimes |\sigma_2\rangle \otimes \ldots \otimes |\sigma_N\rangle$$

within a considered many-body Hilbert space $\otimes_{i=1}^{N} H_i$, which is composed of single particle spaces H_i, by $|\phi\rangle$ [53]. This class of states spans a certain subspace within the full Hilbert space, whose dimension grows by increasing the size of the matrices. The dimension between two neighbouring matrices is called bond dimension. At the heart of an efficient MPS formulation lies the truncation of the bond dimension by keeping only the relevant correlations in the sense of maximizing the entanglement content of a considered bond by a (truncated-) Schmidt decomposition. This works especially well for one dimensional models [54], but is not exclusively restricted to them [55–57]. This truncation procedure tries to keep the matrix sizes slim and numerically accessible, but also to capture the most relevant correlations in the above sense.

Over the past decades a number of algorithms have been developed to find the MPS representation of quantum states or perform operations on them. For example density matrix renormalization group was developed [58–60] to find the ground state of a given many-body system or the ancilla method also known as purification to deal with mixed states and finite temperature calculations [61] within an MPS formulation. Additionally a number of real or imaginary time evolution schemes for states in the MPS representation are available, like the time-evolving block decimation [62–64] or, more recently, the so called tangent space methods, which are based on the time-dependent variational principle (TDVP) [50, 65–67]. Time evolution usually leads to an increasing entanglement entropy and therefore vastly growing bond dimension [68], limiting the accessible time scales [69].

In this study, temperature effects are taken into account by employing the purification method to represent the density matrix of the system as a pure MPS in an enlarged Hilbert space, as described in [49, 61]. We arrange the local Hilbert spaces for the MPS treatment following [51, 70] according to their phonon frequencies and truncate the infinite dimensional Hilbert space of each of the phonon modes to the subspace spanned by the set

$$\{|n_i\rangle\}_{n_i=0,\ldots,N_b(i)},$$

where n_i denotes the occupation number of mode *i*. We estimate the 'maximally' involved occupation numbers by

$$N_b(i) = \max\left\{n_b(\hbar\omega_i) + 2\sqrt{\mathrm{Var}(i)}, 5\right\},$$
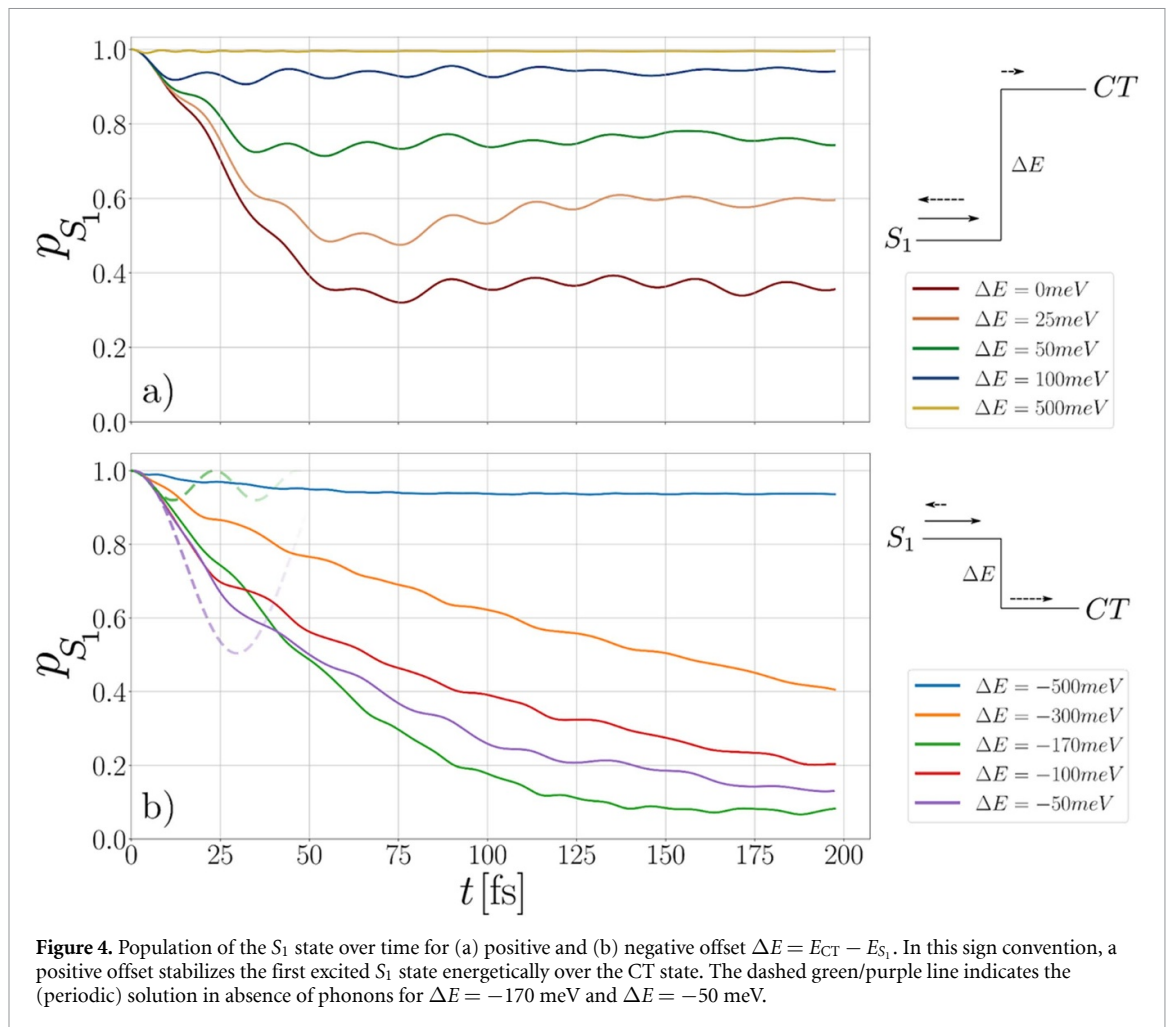
where $n_b(\hbar\omega_i) = \langle n_i \rangle = \frac{1}{\exp(\beta\hbar\omega_i)-1}$ is the Bose–Einstein-distribution (BED) of mode *i* and $\mathrm{Var}(\hbar\omega_i) = \langle n_i^2 \rangle - \langle n_i \rangle^2 = \frac{\beta\hbar\omega_i}{(\exp(\beta\hbar\omega_i)-1)^2}$, the variance of the BED. This truncation procedure reproduces the statistics for the decoupled modes with $\hbar\omega_i \gtrsim k_B T$ very accurately. The modes with $\hbar\omega_i \lesssim k_B T$ are strongly thermally populated, but this choice still reproduces the statistics up to a few per thousand. The computational expense to correctly reproduce the BED in this regime is enormous, and we therefore stick to the presented scheme. As the electron–phonon coupling is not very large for all the considered modes, the minimum dimensionality of the local Hilbert spaces also suffices to capture the coherent polaronic processes.

To perform the time evolution we use a hybrid version of the TDVP code from [71]. We find that it is necessary to make use of the global subspace expansion for the TDVP algorithm as described in [72] and implemented in [71], to sufficiently fast generate the long-range entanglement within the initial product state. We first perform two iterations of the global subspace expansion, then we make one time step of the two-site TDVP version of the code, to dynamically evolve the bond dimension using the truncation threshold 10^{-10} for the singular values. After this, 20 time steps of the single-site version to limit the computational expense of the calculation are performed, and the process restarted. We take a time step of $\Delta t \approx 0.2\,\mathrm{fs}$ for all the calculations and use the ITensor software library [73] for the MPS quantum dynamics (MPS-QD) simulations.

3. Results

3.1. Population dynamics
From the MPS-QD simulations, we obtain the time resolved population of the S_1 state (figure 4). Here we restrict ourselves to times up to 200 fs, since on this scale the dissociation into free carriers or recombination

Figure 4. Population of the S_1 state over time for (a) positive and (b) negative offset $\Delta E = E_{CT} - E_{S_1}$. In this sign convention, a positive offset stabilizes the first excited S_1 state energetically over the CT state. The dashed green/purple line indicates the (periodic) solution in absence of phonons for $\Delta E = -170$ meV and $\Delta E = -50$ meV.

is experimentally found to be not important [38]. Depending on the energetic offset ΔE between the excitonic S_1 state (often termed singlet state) and the CT state, we observe different behaviours.

Let us start the discussion by considering large $|\Delta E|$. For this regime, the behaviour can already be understood by completely neglecting the vibrations for a moment. In this case the Hamiltonian reduces to H_{el}. For large $|\Delta E|$ the electronic eigenstates of H_{el} have a more localized character than for small $|\Delta E|$. The localized initial state is therefore close to an eigenstate (weak hybridization for $V/|\Delta E| \ll 1$) and CT is limited and becomes more and more suppressed with increasing $|\Delta E|$, preventing a significant population of the CT state. This behaviour can be observed for the cases of $\Delta E > 100$ meV and $\Delta E < -400$ meV. The asymmetry between positive and negative offsets is further discussed below.

In the opposite limit of a small $|\Delta E|$ (i.e. $\Delta E \approx V$) and still neglecting the phonons, the electronic eigenstates are delocalized over the system, which leads to an ultrafast population of the CT state. On short time scales this kinetically driven behaviour can be observed for a rather large energy range around zero-driving (i.e. 25 meV $\gtrsim \Delta E \gtrsim -50$ meV, cf figure 4). However here the purely electronic picture has its limit since the delocalized eigenstates would lead to a complete back transfer into the S_1 state after one period, which is absent in the electron–phonon coupled system. This is because energy is dissipated into the phonon subsystem over time, which is accompanied by the activation of more strongly coupled phonon-modes in the dynamics. As a result, the electron transfer is slowed down, thus favouring the localization of the exciton at the acceptor site. These dissipation and polaron formation processes make charge separation possible, because they hinder the back transfer and trap a large fraction of the electron in the CT state. On longer time scales this leads to a (weakly modulated) steady state hybridization between the S_1 and CT states which depends weakly on the initial state.

Beyond this general picture, that phonon modes can assist the charge separation, there are variations in the impact of the molecular vibrations on the electron dynamics, which we want to discuss now. From the purely electronic picture discussed above one could expect, that by decreasing the driving from $|\Delta E| \approx 0$ meV, the charge separation behaviour should slow down. However we find a different behaviour, which highlights the general importance of the vibrations for the CT in a regime around $\Delta E = -170$ meV
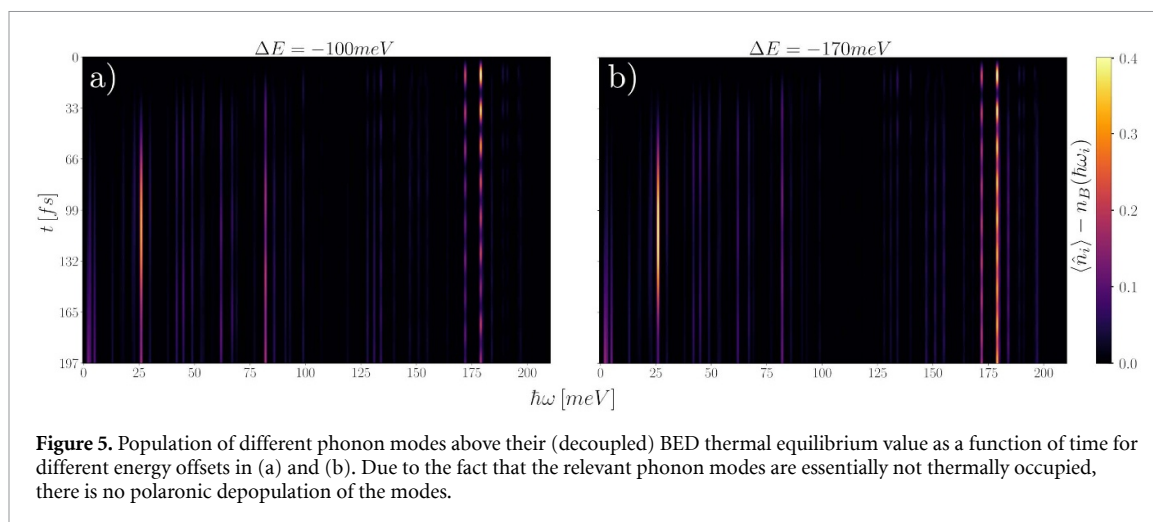
Figure 5. Population of different phonon modes above their (decoupled) BED thermal equilibrium value as a function of time for different energy offsets in (a) and (b). Due to the fact that the relevant phonon modes are essentially not thermally occupied, there is no polaronic depopulation of the modes.

(green curve in figure 4(b)). Here we observe unexpectedly fast and extensive transfer, as compared to the bare electronic picture and to driving energies $\Delta E > -170$ meV. In particular at $\Delta E = -170$ meV we see that at small times the electron transfer is not kinetically driven because it is almost absent when the vibrations are turned off in the simulations (dashed green curve in figure 4(b)). In contrast, the presence of the vibrations enables an alternative relaxation route. In order to rationalize this, we compare the interaction of the vibrations and the charge for $\Delta E = -170$ meV and $\Delta E = -100$ meV, by monitoring their phonon mode occupation numbers as depicted in figure 5.
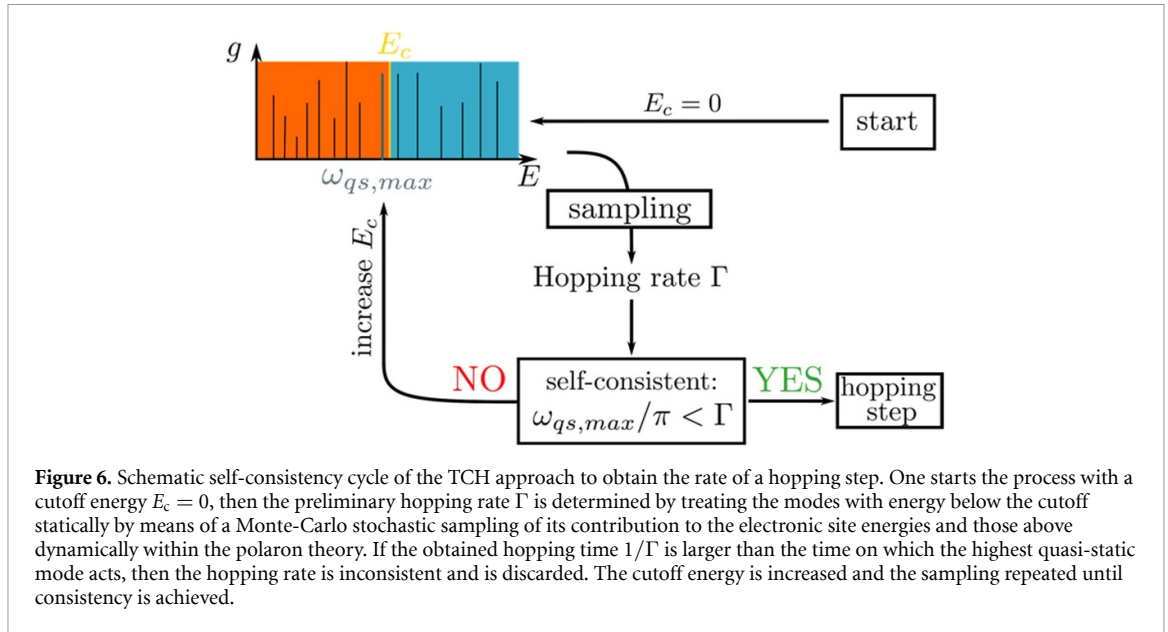
Values exceeding the numbers according to the BED (that are calculated as $\langle \widehat{n}_i \rangle - n_B$) are relevant here and indicate their non-equilibrium population and their involvement in the polaron formation at the donor or acceptor. The occupation of these modes oscillates periodically and the intensity is reduced during the transfer process as less electronic density couples to the phonons at the specific site. The emission of phonons for relaxation reasons, however, interferes with the coherent electron transfer processes, such that the oscillations are blurred out. For $\Delta E = -100$ meV one finds that the phonon dynamics is mostly governed by the polaronic oscillations. Blurring is present only to a limited degree, meaning that charge separation in this case is mostly by kinetics. This is in accordance with figure 3: The PC[70]BM modes around $\hbar\omega_i = 100$ meV couple only weakly to the electronic degree of freedoms, making any single-phonon relaxation processes unlikely. Any relaxation process that involves a larger number of phonons has a smaller amplitude and is therefore slower.

In contrast to that, the case of $\Delta E = -170$ meV shows strong blurring characteristics of the most strongly coupled modes around $\hbar\omega_i = 175$ meV (figure 5(b)), and also for a mode around 85 meV. The former mode energy closely matches the energy difference $\sqrt{(\Delta E)^2 + 4V^2}$ of the bare electronic states, while the latter is a factor of two smaller. The blurring characteristics can hence be identified as single respectively double phonon emission processes, which explains why the charge separation in this case is more rapid than in the case of $\Delta E = -100$ meV. This relaxation route also explains the previously mentioned asymmetry in the localization regime: For a large negative offset, relaxation via phonon emission is possible, whereas for a positive offset it is an on-shell energetically forbidden process.

This overall behaviour shows that for systems experiencing a moderate driving force the dissipation of energy to phonons is essential for charge separation. It also hints towards a rule of thumb (design rule): A matching driving energy with the most strongly coupled phonon modes is beneficial for the charge separation, if zero driving is not in reach.

3.2. CT rates and comparison to the TCH approach

Semiclassical hopping theories for charge transport (in different variants) are widespread and accepted in the field of organic disordered materials [27, 74] or for electron transfer reactions in physical chemistry [75] because of the ease of use and the very low computational expenses for the estimation of CT rates and transport coefficients. In absence of a clear-cut validity range for their application in the field of organic solar cells, a realistic benchmark simulation is useful and we try to close this gap by comparing one of the newly developed hopping theories, the TCH approach, to the fully quantum mechanical MPS-QD and analyse the overall consistency of the description. In order to compare the MPS-QD with the TCH approach we investigate the time scale on which this CT process takes place. The definition of the CT time for any quantum dynamical simulation is not unique. A possible definition of the transfer time (and therefore a

Figure 6. Schematic self-consistency cycle of the TCH approach to obtain the rate of a hopping step. One starts the process with a cutoff energy $E_c = 0$, then the preliminary hopping rate Γ is determined by treating the modes with energy below the cutoff statically by means of a Monte-Carlo stochastic sampling of its contribution to the electronic site energies and those above dynamically within the polaron theory. If the obtained hopping time $1/\Gamma$ is larger than the time on which the highest quasi-static mode acts, then the hopping rate is inconsistent and is discarded. The cutoff energy is increased and the sampling repeated until consistency is achieved.
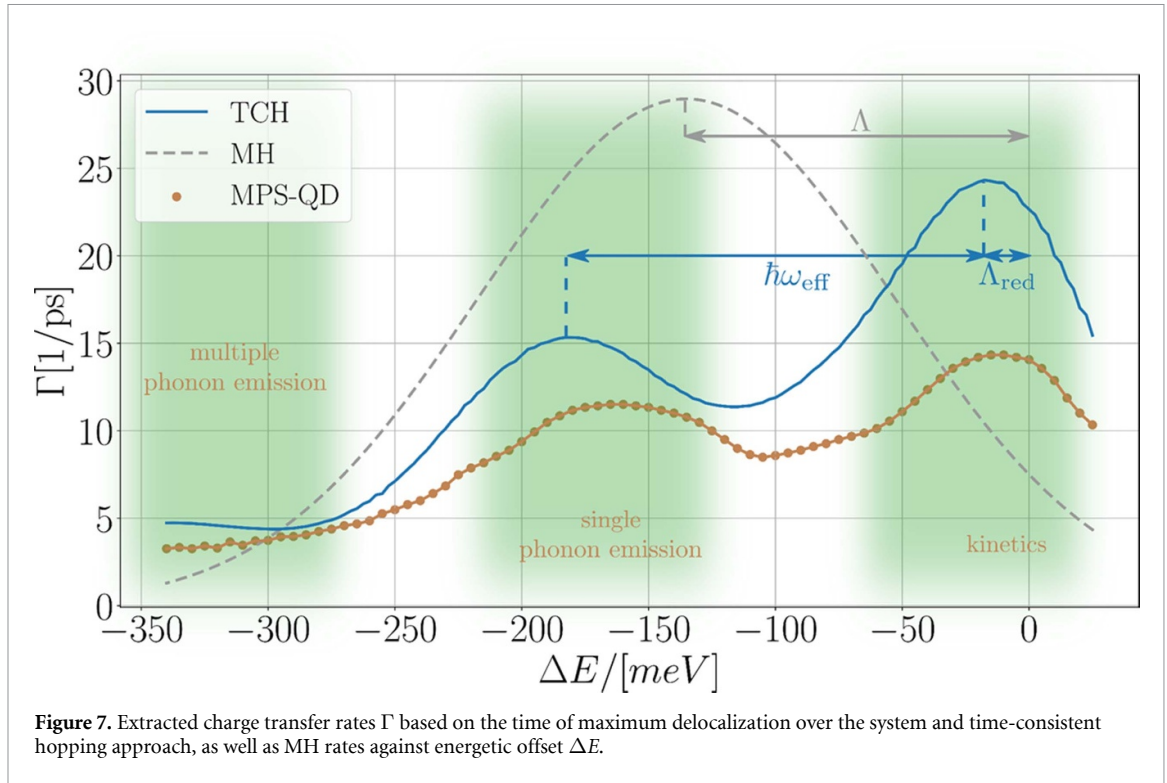
corresponding rate) is intimately related to the hopping picture of charge transport between two states. Indeed, a single-step CT describes that at a given point in time a carrier is at one specific site and at the next moment in time at another site. In this description, the complex process of the transfer is coarse grained to a single event (or a sequence of independent events), characterized by a specific time on which this event happens. While for hopping models the transfer time is unequivocally defined, we discuss further below how we measure it in the quantum dynamics simulations after first introducing the TCH approach.

Within the class of hopping models in the literature different expressions and motivations for the derivation of CT rates are given. Some are based on thermodynamic considerations [27, 28], others are derived from Fermi's golden rule calculations, second-order cumulant expansion [76, 77] or Kubo's formula [30]. Each of the individual approaches focuses on one of the specific aspects of the transfer process, e.g. MH theory considers a thermal activation barrier, while approaches based on Fermi's golden rule follow (by their starting point) a perturbative quantum mechanical route, by including specific (coherent) processes.

In the TCH approach, with which we compare, the obtained charge separation rates are based on the separation of the phonon modes into dynamic ones, which contribute to the polaronic dressing of the coupled carrier and static ones providing an effective electronic disorder landscape [30]. In contrast to MH and LJH theories, the TCH approach determines in a self-consistent fashion, which modes have to be treated dynamically and which ones are static on the time scale on which the hopping process takes place. This is done by dividing the mode spectrum into three energy regimes: a completely dynamical energy range, whose modes are casted into an effective high energy mode ω_{eff}, a low-energy window of dynamic modes and quasi-static modes of even smaller energy. The dynamic modes that lie in the low-energy window contribute to a reduced reorganization energy Λ_{red} and the quasi static modes are treated within a stochastic sampling. The energy E_c separating the low-energy dynamic and quasi-static modes is determined self-consistently, by enforcing that the hopping time is faster than the quasi-static modes, but slower, than the low-energy dynamic modes (cf figure 6).

As mentioned above, the fully quantum mechanical non-equilibrium situation of the problem studied here within the MPS methodology makes it hard to extract a CT time based on the definitions mentioned previously. We therefore define it independently of the common concepts, as we found that these fail in this purely quantum mechanical setting. Building on the picture provided in [78], that short-lived delocalized band-like states are responsible for the charge separation, we define the CT time as twice the time where the electronic part of the many-body wave function is completely delocalized over the system for the first time. Indeed, this is consistent with the hopping picture of a full CT by identifying the time of 'half of the hopping process' with the delocalization time. To extract the concrete transfer time scale we consider the inverse participation ratio (IPR)

$$\Pi(t) = \frac{1}{p_{S_1}^2 + (1 - p_{S_1})^2}.$$

.

Figure 7. Extracted charge transfer rates Γ based on the time of maximum delocalization over the system and time-consistent hopping approach, as well as MH rates against energetic offset ΔE.

$\Pi(t)$ is a measure for the (de-)localization of a many-body wave function over the system. The IPR has the two trivial limits of being 1 if the state under consideration is completely localized and being 2 if the state is completely delocalized. We take the time t_{trans} of the electron transfer to be determined by

$$\Pi(t_{\text{trans}}/2) = 2,$$

which yields the transfer rate

$$\Gamma = 1/t_{\text{trans}},$$

which is related to the half time. It should be mentioned that the application of this definition is adapted to the behaviour where there is a significant 'irreversible' transfer of density. For this reason we restrict the comparison to those cases, where a significant amount of the exciton wave function is transferred to the CT state, meaning that within the first 200 fs more than 50% of the charge density have been transferred into the CT state (cf figure 4). We find that this is the case for $-340\,\text{meV} \leqslant \Delta E \leqslant 25\,\text{meV}$.

Figure 7 shows the resulting transfer rates obtained by the MPS-QD in comparison to the hopping rates obtained by TCH [30] and by the MH theory. We find that the TCH approach yields higher, but consistent absolute values with the MPS-QD over the full range of energetic offsets considered. In addition, they give rise to a very similar driving-energy dependence of the extracted rates. The fastest CT rate for the TCH and the MPS-QD is observed close to zero driving. The MPS-QD reveals that this can be traced back to the large overlap between the bare electronic eigenstates, which results in kinetic behaviour at short time scales.

The TCH ansatz predicts an increase of the rate with periodicity $\hbar\omega_{\text{eff}}$, where ω_{eff} is the frequency that is defined as an effective dynamic mode formed from the high-energy phonons [30]. This is corroborated by the results of the phonon-assisted relaxation observed in the MPS-QD, which increases the transfer rate in the range, where the exciton can efficiently relax via phonon-emission. A second (barely) visible replica structure at the very left of figure 7 ($\Delta E < -300$ meV) corresponds to higher order (= multiple phonon emission) processes, which explains on the one hand the reduced transfer rate compared to the first replica structure and, on the other hand, that the transfer rate does not drop completely at strong driving force, i.e. beyond $\Delta E = -220$ meV.

Although the correct order of magnitude is predicted by the MH theory, it misses essentially all of the features found in the other two approaches: The replica structure(s) and the maximum of the rate close to zero driving energy. Furthermore, the overall curve shape does not match the other two results, which may lead to the conclusion that MH in this case provides only an oversimplified picture of the transport process, despite predicting the correct order of magnitude for the rate.

Despite the apparent similarities between MPS-QD and TCH, there are differences in the obtained transfer rates. The overall curve shape of the MPS-QD and the TCH approach is similar, but not identical. The TCH approach yields larger rates and the maxima are more pronounced than in the MPS-QD, whereas the MPS-QD gives rise to a broader course of the curve. This may be related to the fact that in the TCH approach the effect of all the high-energy modes is collected into a single effective mode, while there is a much larger number of possible phonon-modes for relaxation in the MPS-QD.

Deviations in the absolute value of the rate between the two different theoretical treatments might be caused by the narrow band approximation implicit in the TCH approach, the absence of coherent contributions and by the different underlying definition of the transfer rate which cannot be made fully equivalent. The first aspect could also explain the generally smaller rate obtained by the MPS-QD, as there destructive interference and orthogonality within the phonon subspaces are fully quantum mechanically taken into account. However, overall both approaches predict remarkably matching energy-dependencies of the CT rates, given the differences in the methods Thus they draw a consistent physical picture for the underlying processes. Furthermore, they are consistent with the CT rates obtained in the experimental measurements in [40].

4. Summary and conclusion

In this article we studied the CT process at the interface of a DPP-PC[70]BM solar cell blend system based on a fully quantum mechanical model. Starting from the three step picture of free charge generation in organic photovoltaic systems, an effective Hamiltonian, describing the intermediate time scales between excitation and dissociation of the CT state into free carriers, was proposed. Using this effective Hamiltonian the full quantum dynamics of the excited exciton state $|S_1\rangle$ under the influence of 114 coarse grained phonon modes into the CT state was investigated via the MPS ansatz. We found that for the practically most relevant case of near zero driving energy ΔE, the process of CT is on short time scales governed by the kinetics of the initial state, transferring charge density into the CT state, and is energetically driven by relaxation dynamics at longer time scales. Furthermore, the study revealed that for a moderate driving of the system, an efficient charge separation critically depends on the availability of coupled phonon modes to which excess energy can be transferred to.

In addition, the comparison between the MPS based methodology and the TCH approach yielded surprisingly consistent results, showing that consistently employed analytical limits for the molecular vibrations can capture the most important effects of the electron–phonon coupling.

Data availability statement

All data that support the findings of this study are included within the article (and any supplementary files).

Acknowledgments

ORCID iDs

Raffaele Borrelli ⓘ https://orcid.org/0000-0002-0060-4520
Frank Ortmann ⓘ https://orcid.org/0000-0002-5884-5749

References

[1] Dennler G, Scharber M C and Brabec C J 2009 Polymer-fullerene bulk-heterojunction solar cells *Adv. Mater.* **21** 1323–38
[2] Clarke T M and Durrant J R 2010 Charge photogeneration in organic solar cells *Chem. Rev.* **110** 6736–67
[3] Yan C, Barlow S, Wang Z, Yan H, Jen A K-Y, Marder S R and Zhan X 2018 Non-fullerene acceptors for organic solar cells *Nat. Rev. Mater.* **3** 18003
[4] Hou J, Inganäs O, Friend R H and Gao F 2018 Organic solar cells based on non-fullerene acceptors *Nat. Mater.* **17** 119–28
[5] Li C *et al* 2021 Non-fullerene acceptors with branched side chains and improved molecular packing to exceed 18% efficiency in organic solar cells *Nat. Energy* **6** 605–13

[6] Yu G, Gao J, Hummelen J C, Wudl F and Heeger A J 1995 Polymer photovoltaic cells: enhanced efficiencies via a network of internal donor-acceptor heterojunctions *Science* **270** 1789–91

[7] Chen X K *et al* 2021 A unified description of non-radiative voltage losses in organic solar cells *Nat. Energy* **6** 799–806

[8] Linderl T, Zechel T, Hofmann A, Sato T, Shimizu K, Ishii H and Brütting W 2020 Crystalline versus amorphous donor-acceptor blends: influence of layer morphology on the charge-transfer density of states *Phys. Rev. Appl.* **13** 024061

[9] Classen A *et al* 2019 *Adv. Energy Mater.* **9** 1801913

[10] Vandewal K *et al* 2017 Absorption tails of donor: C60 blends provide insight into thermally activated charge-transfer processes and polaron relaxation *J. Am. Chem. Soc.* **139** 1699–704

[11] Spoltore D *et al* 2018 Hole transport in low-donor-content organic solar cells *J. Phys. Chem. Lett.* **9** 5496–501

[12] Liu J *et al* 2016 Fast charge separation in a non-fullerene organic solar cell with a small driving force *Nat. Energy* **1** 16089

[13] Bässler H and Köhler A 2015 'Hot or cold': how do charge transfer states at the donor–acceptor interface of an organic solar cell dissociate? *Phys. Chem. Chem. Phys.* **17** 28451–62

[14] Few S, Frost J M and Nelson J 2015 Models of charge pair generation in organic solar cells *Phys. Chem. Chem. Phys.* **17** 2311

[15] Deibel C, Strobel T and Dyakonov V 2010 Role of the charge transfer state in organic donor–acceptor solar cells *Adv. Mater.* **22** 4097–111

[16] Vandewal K 2016 Interfacial charge transfer states in condensed phase systems *Annu. Rev. Phys. Chem.* **67** 113–33

[17] Morteani A C, Sreearunothai P, Herz L M, Friend R H and Silva C 2004 Exciton regeneration at polymeric semiconductor heterojunctions *Phys. Rev. Lett.* **92** 247402

[18] Vandewal K *et al* 2014 Efficient charge generation by relaxed charge-transfer states at organic interfaces *Nat. Mater.* **13** 63–68

[19] Panhans M, Hutsch S, Benduhn J, Schellhammer K S, Nikolis V C, Vangerven T, Vandewal K and Ortmann F 2020 Molecular vibrations reduce the maximum achievable photovoltage in organic solar cells *Nat. Commun.* **11** 1488

[20] Qian D *et al* 2018 Design rules for minimizing voltage losses in high-efficiency organic solar cells *Nat. Mater.* **17** 703–9

[21] Jakowetz A C, Böhm M L, Zhang J, Sadhanala A, Huettner S, Bakulin A, Rao A and Friend R H 2016 What controls the rate of ultrafast charge transfer and charge separation efficiency in organic photovoltaic blends *J. Am. Chem. Soc.* **138** 11672

[22] Menke S M, Ran N A, Bazan G C and Friend R H 2018 Understanding energy loss in organic solar cells: toward a new efficiency regime *Joule* **2** 25

[23] Aram T N, Ernzerhof M, Asgari A and Mayou D 2018 Impact of offset energies on the yield of interfacial charge separation in molecular photocells *J. Chem. Phys.* **149** 064102

[24] Cook S, Katoh R and Furube A 2009 Ultrafast studies of charge generation in PCBM:P3HT blend films following excitation of the fullerene PCBM *J. Phys. Chem. C* **113** 2547–52

[25] Nikolis V C *et al* 2020 Field effect versus driving force: charge generation in small-molecule organic solar cells *Adv. Energy Mater.* **10** 2002124

[26] Unger T, Wedler S, Kahle F-J, Scherf U, Bässler H and Köhler A 2017 The impact of driving force and temperature on the electron transfer in donor–acceptor blend systems *J. Phys. Chem. C* **121** 22739–52

[27] Marcus R A 1956 On the theory of oxidation-reduction reactions involving electron transfer. I *J. Chem. Phys.* **24** 966

[28] Marcus R A and Sutin N 1985 Electron transfers in chemistry and biology *Biochim. Biophys. Acta* **811** 265–322

[29] Jortner J 1976 Temperature dependent activation energy for electron transfer between biological molecules *J. Chem. Phys.* **64** 4860

[30] Hutsch S, Panhans M and Ortmann F 2021 Time-consistent hopping transport with vibration-mode-resolved electron-phonon couplings *Phys. Rev. B* **104** 054306

[31] Matyushov D 2009 Nonergodic activated kinetics in polar media *J. Chem. Phys.* **130** 164522

[32] Blumberger J 2015 Recent advances in the theory and molecular simulation of biological electron transfer reactions *Chem. Rev.* **115** 11191–238

[33] Cainelli M and Tanimura Y 2021 Exciton transfer in organic photovoltaic cells: a role of local and nonlocal electron–phonon interactions in a donor domain *J. Chem. Phys.* **154** 034107

[34] Brian D, Liu Z, Dunietz B D, Geva E and Sun X 2021 Three-state harmonic models for photoinduced charge transfer *J. Chem. Phys.* **154** 174105

[35] Bera S, Gheeraert N, Fratini S, Ciuchi S and Florens S 2015 Impact of quantized vibrations on the efficiency of interfacial charge separation in photovoltaic devices *Phys. Rev. B* **91** 041107

[36] Janković V and Vukmirović N 2017 Identification of ultrafast photophysical pathways in photoexcited organic heterojunctions *J. Phys. Chem. C* **121** 19602–18

[37] Nematiaram T, Asgari A and Mayou D 2020 Impact of electron–phonon coupling on the quantum yield of photovoltaic devices *J. Chem. Phys.* **152** 044109

[38] Li G 2015 The influence of polaron formation on exciton dissociation *Phys. Chem. Chem. Phys.* **17** 11553–9

[39] Strong S E and Hestand N J 2020 Modeling nonlocal electron–phonon coupling in organic crystals using interpolative maps: the spectroscopy of crystalline pentacene and 7,8,15,16-tetraazaterrylene *J. Chem. Phys.* **153** 124113

[40] Shivhare R *et al* 2021 Short excited-state lifetimes mediate charge-recombination losses in organic solar cell blends with low charge-transfer driving force *Adv. Mater.* 2101784

[41] Aram T M, Asgari A and Mayou D 2016 Charge separation in organic solar cells: effects of Coulomb interaction, recombination and hole propagation *EPL Europhys. Lett.* **115** 18003

[42] Popp W, Brey D, Binder R and Burghardt I 2021 Quantum dynamics of exciton transport and dissociation in multichromophoric systems *Annu. Rev. Phys. Chem.* **72** 591–616

[43] Baumeier B, Kirkpatrick J and Andrienko D 2010 Density-functional based determination of intermolecular charge transfer properties for large-scale morphologies *Phys. Chem. Chem. Phys.* **12** 11103

[44] Becke A D 1988 Density-functional exchange-energy approximation with correct asymptotic behavior *Phys. Rev. A* **38** 3098

[45] Becke A D 1993 A new mixing of Hartree–Fock and local density-functional theories *J. Chem. Phys.* **98** 1372

[46] Krishnan R, Binkley J S, Seeger R and Pople J A 1980 Self-consistent molecular orbital methods. XX. A basis set for correlated wave functions *J. Chem. Phys.* **72** 650–4

[47] Malagoli M, Coropceanu V, Da Silva Filho D A and Brédas J L 2004 A multimode analysis of the gas-phase photoelectron spectra in oligoacenes *J. Chem. Phys.* **120** 7490–6

[48] Ortmann F, Radke S, Günther A, Kasemann D, Leo K and Cuniberti G 2015 Materials meets concepts in molecule-based electronics *Adv. Funct. Mater.* **25** 1933

[49] Schollwöck U 2011 The density-matrix renormalization group in the age of matrix product states *Ann. Phys.* **326** 96–192

[50] Paeckel S, Köhler T, Swoboda A, Manmana S R, Schollwöck U and Hubig C 2019 Time-evolution methods for matrix-product states *Ann. Phys.* **41** 167998

[51] Borrelli R and Gelin M F 2021 Finite temperature quantum dynamics of complex systems: integrating thermo-field theories and tensor-train methods *WIREs Comput. Mol. Sci.* e1539

[52] Weichselbaum A, Verstraete F, Schollwöck U, Cirac J I and Von Delft J 2009 Variational matrix-product-state approach to quantum impurity models *Phys. Rev. B* **80** 165117

[53] Borrelli R 2018 Theoretical study of charge-transfer processes at finite temperature using a novel thermal Schrödinger equation *Chem. Phys.* **515** 236–41

[54] Eisert J, Cramer M and Plenio M B 2010 Colloquium: area laws for the entanglement entropy *Rev. Mod. Phys.* **82** 277–306

[55] White S R and Scalapino D J 1998 Energetics of domain walls in the 2D t−J model *Phys. Rev. Lett.* **81** 3227

[56] Rommer S, White S R and Scalapino D J 2000 Phase separation in t-J ladders *Phys. Rev. B* **61** 13424–30

[57] Stoudenmire E M and White S R 2012 Studying two-dimensional systems with the density matrix renormalization group *Annu. Rev. Condens. Matter Phys.* **3** 111–28

[58] White S R 1992 Density matrix formulation for quantum renormalization groups *Phys. Rev. Lett.* **69** 2863–6

[59] White S R 1993 Density-matrix algorithms for quantum renormalization groups *Phys. Rev. B* **48** 10345–56

[60] Verstraete F, Porras D and Cirac J I 2004 Density matrix renormalization group and periodic boundary conditions: a quantum information perspective *Phys. Rev. Lett.* **93** 227205

[61] Verstraete F, Garcia-Ripoll J J and Cirac J I 2004 Matrix product density operators: simulation of finite-temperature and dissipative systems *Phys. Rev. Lett.* **93** 207204

[62] Vidal G 2003 Efficient classical simulation of slightly entangled quantum computations *Phys. Rev. Lett.* **91** 147902

[63] White S R and Feiguin A E 2004 Real-time evolution using the density matrix renormalization group *Phys. Rev. Lett.* **93** 076401

[64] Daley A J, Kollath C, Schollwöck U and Vidal G 2004 Time-dependent density-matrix renormalization-group using adaptive effective Hilbert spaces *J. Stat. Mech: Theory Exp.* P04005

[65] Haegeman J, Cirac J I, Osborne T J, Pižorn I, Verschelde H and Verstrate F 2011 Time-dependent variational principle for quantum lattices *Phys. Rev. Lett.* **107** 070601

[66] Haegeman J, Osborne T J and Verstraete F 2013 Post-matrix product state methods: to tangent space and beyond *Phys. Rev. B* **88** 075133

[67] Haegeman J, Lubich C, Oseledets I, Vandereycken B and Verstraete F 2016 Unifying time evolution and optimization with matrix product states *Phys. Rev. B* **94** 165116

[68] Perales Á and Vidal G 2008 Entanglement growth and simulation efficiency in one-dimensional quantum lattice systems *Phys. Rev. A* **78** 042337

[69] Gobert D, Kollath C, Schollwöck U and Schütz G 2005 Real-time dynamics in spin-1/2 chains with adaptive time-dependent density matrix renormalization group *Phys. Rev. E* **71** 036102

[70] Borrelli R and Gelin M F 2016 Quantum electron-vibrational dynamics at finite temperature: thermo field dynamics approach *J. Chem. Phys.* **145** 224101

[71] Yang M and Fishman M ITensor implementation of TDVP code used in [72] (Version downloaded from 12 05 2021) (available at: https://github.com/ITensor/TDVP) (Accessed 12 May 2021)

[72] Yang M and White S R 2020 Time-dependent variational principle with ancillary Krylov subspace *Phys. Rev. B* **102** 094315

[ ] Fishman M, White S R and Stoudenmire E M 2020 The ITensor software library for tensor network calculations (arXiv:2007.14822)

[74] Miller J R, Calcaterra L T and Closs G L 1984 Intramolecular long-distance electron transfer in radical anions. The effects of free energy and solvent on the reaction rates *J. Am. Chem. Soc.* **106** 3047–9

[75] Lu N, Li L, Banerjee W, Sun P, Gao N and Liu M 2015 Charge carrier hopping transport based on Marcus theory and variable-range hopping theory in organic semiconductors *J. Appl. Phys.* **118** 045701

[76] Borrelli R and Peluso A 2015 Quantum dynamics of radiationless electronic transitions including normal modes displacements and Duschinsky rotations: a second-order cumulant approach *J. Chem. Theory Comput.* **11** 415–22

[77] Landi A, Borrelli R, Capobianco A, Velardo A and Peluso A 2018 Hole hopping rates in organic semiconductors: a second-order cumulant approach *J. Chem. Theory Comput.* **14** 1594–601

[78] Bakulin A, Rao A, Pavelyev V G, van Loosdrecht P H M, Pshenichnikov M S, Niedzialek D, Cornil J, Beljonne D and Friend R H 2012 The role of driving energy and delocalized states for charge separation in organic semiconductors *Science* **16** 1340–4